Journal of Environmental Chemical Engineering 14 (2026) 120907

Contents lists available at ScienceDirect

Journal of Environmental Chemical Engineering

journal homepage: www.elsevier.com/locate/jece

Waste-to-waste strategy for lithium-ion battery recycling: Biosorption of Ni, Co and Mn using bergamot pomace

Salvatore Giovanni Michele Raccuia [a,1], Davide Lascari [b,1], Roberto Di Pietro [c], Stiven López Guzmán [d,e], Emilie Bekaert [d], Nicola Muratore [b], Emanuele Gucciardi [d], Salvatore Cataldo [b], Alberto Pettignano [b], Paola Cardiano [a,*], Gabriele Lando [a]

[a] Dipartimento di Scienze Chimiche, Biologiche, Farmaceutiche e Ambientali, Università degli Studi di Messina, Viale Ferdinando Stagno d'Alcontres 31, Messina 98166, Italy
[b] Dipartimento di Fisica e Chimica– Emilio Segré, Università degli Studi di Palermo, Viale delle Scienze, Palermo 90128, Italy
[c] Dipartimento di Ingegneria, Università degli Studi di Messina, Contrada Di Dio, Messina 98168, Italy
[d] Center for Cooperative Research on Alternative Energies (CIC energiGUNE), Basque Research and Technology Alliance (BRTA), Alava Technology Park, Albert Einstein 48, Vitoria-Gasteiz 01510, Spain
[e] Chemical and Environmental Engineering Department, Faculty of Science and Technology, University of the Basque Country, UPV/EHU, BoSarriena s/n, Leioa 48940, Spain

ARTICLE INFO

Keywords:
Lithium-ion batteries recycling
Biosorbent
Critical metals recovery
Sustainable materials
Hydrometallurgy
Tecno-economic assessment

ABSTRACT

The growing demand for lithium-ion batteries (LIBs) in electric mobility and energy storage systems necessitates sustainable recycling solutions. This study presents a proof-of-concept for the recovery of critical metals, *i.e.* Nickel (Ni), Manganese (Mn), and Cobalt (Co), from spent LIBs cathodes using an agri-food waste biomass - bergamot pomace (BP) - as a biosorbent. Due to the complexity of the real cathode matrix, a solid experimental strategy with three levels of increasing complexity was designed: starting with single-metal adsorption experiments, moving to a multicomponent synthetic solution reproducing the cationic composition of the cathode, and finally testing a solution obtained through acid leaching of an actual spent cathode. The experimental data were interpreted through a thermodynamic approach, focusing on adsorption isotherm parameters such as affinity constants and maximum adsorption capacities. BP exhibited a total sorption capacity of approximately 0.7 mmol g^{-1} on real leachates, with a high affinity for Ni, Mn, and Co in diluted solutions (< 30 mg dm^{-3}), indicating strong potential for use in secondary recovery steps. This approach improves metal recovery efficiency, potentially compensating for cation losses in conventional methods, and aligns with circular economy principles by valorizing organic waste. The environmental and economic implications of BP production were also evaluated, focusing on energy consumption, global warming potential (GWP), and production costs under laboratory and projected industrial conditions to assess its sustainability as a complementary step in LIBs recycling workflows. These results demonstrate the viability of BP as a low-cost and bio-based material for greener recycling strategies.

1. Introduction

The global shift towards renewable energy underscores the urgent need for efficient and durable energy storage systems that can meet growing demand while minimizing the environmental impact of conventional power sources. Lithium-ion batteries (LIBs), owing to their high energy density and long operational lifespan, have become the preferred storage technology for a wide range of applications, including grid-scale energy systems and electric vehicles [1,2].

As essential tools for decarbonization in both the energy and transportation sectors, LIBs play a central role in the transition to a more sustainable energy landscape. However, the rapid increase in LIB

* Corresponding author.
E-mail addresses: saraccuia@unime.it (S.G.M. Raccuia), davide.lascari@unipa.it (D. Lascari), robdipietro@unime.it (R. Di Pietro), slopez@cicenergigune.com (S. López Guzmán), ebekaert@cicenergigune.com (E. Bekaert), nicola.muratore@unipa.it (N. Muratore), egucciardi@cicenergigune.com (E. Gucciardi), salvatore.cataldo@unipa.it (S. Cataldo), alberto.pettignano@unipa.it (A. Pettignano), pcardiano@unime.it (P. Cardiano), glando@unime.it (G. Lando).
[1] These authors share first authorship.

https://doi.org/10.1016/j.jece.2025.120907
Received 29 October 2025; Received in revised form 15 December 2025; Accepted 25 December 2025
Available online 26 December 2025

production, driven by the widespread electrification and the expansion of renewable energy infrastructure, is expected to lead to a significant accumulation of end-of-life (EoL) batteries in the near future. This emerging waste stream presents serious environmental and logistical challenges, emphasizing the urgent need for effective recycling strategies [3,4]. Recycling has been identified as a key solution, focusing on the recovery of valuable materials, particularly from the cathode, which accounts for approximately 31 % of a battery cell's mass and 33 % of its total value [5].

Spent LIBs contain valuable metals such as lithium (Li), cobalt (Co), and nickel (Ni), which are not only economically critical but also environmentally hazardous if improperly managed [6]. The uncontrolled disposal of LIBs can lead to soil contamination, fire risk, and toxic exposure, particularly due to cobalt, posing serious environmental and health threats. Recovering these metals is therefore essential for both environmental protection and resource conservation. Incorporating recovered metals back into the production cycle reduces dependence on primary raw material extraction and contributes to minimizing waste, thereby advancing circular economy principles in improved manufacturing [7].

Moreover, forthcoming European regulations will mandate recovery targets of 80 % for lithium and 95 % for cobalt and nickel by 2031 [8], underscoring the urgency of developing efficient and scalable recycling technologies aligned with sustainability goals.

The current industrial recycling methods for LIBs mainly focus on pyrometallurgical and hydrometallurgical processes [9]. Pyrometallurgical methods involve high-temperature treatments to recover metals such as cobalt and nickel. However, these processes are highly energy-intensive, often resulting in substantial lithium losses and producing hazardous by-products, which limits their overall efficiency and environmental compatibility [10,11]. In contrast, hydrometallurgical approaches employ aqueous leaching and chemical separation methods, offering higher metal recovery rates and reduced environmental impact. These methods are generally considered more sustainable and adaptable to large-scale LIB recycling [12–14]. Nonetheless, both approaches present challenges, including high chemical consumption, complex waste management, and difficulties in selectively recovering high-purity metals.

Direct recycling has emerged as a promising alternative, aiming to retain the structural and chemical integrity of cathode materials without requiring extensive decomposition and purification steps [15]. This approach significantly reduces energy consumption and environmental impacts of the recycling processes [16,17]. However, practical implementation remains limited due to the complexity of separating battery components, the removal of impurities and the high cost associated with preserving material integrity at scale [18].

To overcome these limitations, research has increasingly focused on the use of bio-based sorbents, *i.e.* natural materials derived from biomass, which possess inherent ion-exchange and adsorption capabilities. These materials offer a sustainable strategy for selectively recovering metal cations from the leachates of spent battery cathodes. Among them, agricultural byproducts such as fruit pomace have attracted particular interest due to their abundance, renewability, and functional surface chemistry [19–23].

In particular, fruit pomace contains active groups capable of coordinating metal ions, making it an effective, low-cost sorbent for recovering lithium, cobalt, and nickel from aqueous solutions [24–27]. Furthermore, some of these materials exhibit favorable redox properties, thus participating in reduction-oxidation reactions relevant to metal separation and recovery [28,29].

Biomass-based sorbents offer several advantages, including low cost, renewability, and the ability to be regenerated and reused with minimal loss in efficiency, making them an environmentally and economically viable option for large-scale applications [28]. Recent studies have focused on optimizing extraction conditions and enhancing selectivity through tailored sorbent design [30,31]. Recent research has expanded the use of agricultural wastes as green reagents within sustainable hydrometallurgical processes for the recovery of NMC metals. A notable development concerns biomass-derived reducing agents capable of replacing conventional reductants in leaching systems. For example, tea waste, rich in lignocellulose and polyphenolic compounds, was shown to fully leach Ni and Mn and recover approximately 90 % of Co under optimized H_2SO_4 conditions [32]. Likewise, sugarcane molasses has recently been demonstrated to be an efficient reductant in methanesulfonic media, enabling dissolution yields above 85–88 % for Ni, Co and Mn [33]. In addition to their reductive behavior, several agro-wastes have also been investigated as low-cost adsorbents for metal removal from hydrometallurgical leachates or wastewater. Rice husk, a silica-rich lignocellulosic residue, continues to attract attention for its adsorption properties toward transition metals, with recent work emphasizing its relevance compared to other lignocellulosic materials [34]. Despite the growing interest in bio-based sorbents, their application to lithium-ion battery recycling remains extremely limited, and no previous study has investigated BP for the recovery of Ni^{2+}, Co^{2+} and Mn^{2+} from NMC-type cathode leachates. In this context, bergamot pomace (BP), a byproduct of the *citrus* juice and essential oil industry, has emerged as a promising biosorbent. Rich in polyphenols, flavonoids, and other phytochemicals [35,36], BP has demonstrated metal-binding capabilities, as shown, for instance, in works on Cd^{2+} and lanthanides recovery [37,38]. Based on this, the aim of the study is to evaluate the possibility of employing BP as a sorbent after the hydrometallurgical step to improve the efficiency of the global recovery process. According to Gebeyehu et al. [13], the recovery of lithium, cobalt, nickel and manganese via hydrometallurgical processes from spent LIBs is generally high but not complete, with recovery efficiency ranging from $\sim$ 80 to $>$ 99 %, depending on the specific metal cation, on the leaching procedure, and on the recovery mechanism (*e.g.*, electrodeposition, precipitation).

This study presents a novel waste-to-waste strategy by integrating BP as a low-cost and eco-friendly sorbent material into the hydrometallurgical recycling of spent LIBs, contributing to enhancing the sustainability of battery recycling practices. Here several advancements are introduced: a) the first evaluation of BP as a waste-derived sorbent for hydrometallurgical LIB leachates; b) a three-level adsorption strategy progressing from single-cation to synthetic multicomponent solutions and finally to a real NMC622 leachate; c) mechanistic insights of the enhanced adsorption observed in real leachates, considering ionic strength and colloidal carbon originating from the cathode; and d) an integrated techno-economic and life-cycle inventory assessment of BP production, enabling direct comparison with commercial sorbents. Together, these contributions establish BP as a novel and sustainable waste-to-waste material for complementary recovery steps in LIB recycling workflows.

The proof of concept was assessed through three different sets of isotherm batch experiments in which approximately 20 mg of dried BP was contacted with aqueous feed solutions containing target metal cations at varying concentrations to evaluate the effect of different solid-to-liquid ratios. In the first experiment a leachate obtained from a real spent cathode powder was used as feed solution, in the second set, four mono-elemental synthetic solutions (one for each of the target cations, namely lithium, nickel, cobalt and manganese) were employed. In contrast, in the third set of experiments, a mixed synthetic solution simulating the typical composition of a real cathode leachate was adopted.

In addition to evaluating the sorption performance of BP, the study assesses the environmental and economic aspects of its production, focusing on energy consumption, the global warming potential (GWP), and production costs under both laboratory and industrial conditions. This provides a broader understanding of the sustainability and scalability of integrating BP into existing recycling processes.

2. Materials and methods

2.1. Chemicals and experimental procedures

A spent Routejade SLPB98106100 commercial battery (nominal capacity: 10 Ah) was employed in this study. The cell was disassembled inside a Jacomex® glove box under a controlled inert atmosphere (O_2 < 2 mg dm^{-3}, H_2O < 0.5 mg dm^{-3}) to avoid undesired reactions. The positive electrode, consisting of a layered oxide with nominal composition $LiNi_{0.6}Mn_{0.2}Co_{0.2}O_2$ (NMC622), was harvested for further processing. To isolate the active material, the electrode was cut into small pieces and treated with heated ethylene glycol under constant stirring for 1 h, promoting delamination of the coating layer. The detached material was collected, washed with deionized water, dried, and ground into a fine powder, hereafter referred to as RJ-EtGly.

For the leaching step, approximately 0.350 g of RJ-EtGly was mixed with 10 cm^3 of concentrated nitric acid (HNO_3, ≥ 65 % w/w, ~15 mol dm^{-3}, Sigma Aldrich) and 9 cm^3 of 3 % hydrogen peroxide (H_2O_2, ~ 0.89 mol dm^{-3}, Merck) in a closed 50 cm^3 flask under heating until the solid was completely dissolved. The mixture was then diluted to 30 cm^3 with decarbonated water and subjected to ultrasonic treatment at around 40 °C, with magnetic stirring to enhance dissolution. The resulting solution was centrifuged at 6000 rpm for 1 h and then filtered through a 0.45 μm membrane (SPHEROS) to remove any remaining solid residues. The pH of the filtered solution was adjusted to ~ 5.0 using a standard NaOH solution (~ 0.1 mol dm^{-3}), and the volume was brought to 250 cm^3 with deionized water in a volumetric flask to obtain the ***mother solution*** used in subsequent experiments. The precipitation of the valuable metals during pH adjustment can be considered negligible. A distribution diagram built at 25 °C, using the hydrolysis constants reported in the JESS database, confirmed that, in the ***mother solution*** conditions, the hydrolytic behaviour of the three metal cations becomes relevant at pH > 6. This protocol was found to be suitable based on preliminary solubility tests.

Elemental concentrations in the mother solution were determined by Inductively Coupled Plasma – Optical Emission Spectroscopy (ICP-OES) using a PerkinElmer Model Optima 2100 equipped with an AS-90 autosampler and WinLab32 software. The ICP-OES operating conditions were: RF power of 1.3 kW, plasma-gas flow rate of 15 dm^3 min^{-1}, sheath-gas flow rate of 0.2 dm^3 min^{-1}, and nebulizer flow rate of 0.8 dm^3 min^{-1}. The wavelengths employed for analysis were 460.286 nm for lithium, 257.61 nm for manganese, 228.616 nm for cobalt, and 231.604 nm for nickel. Calibration curves were prepared over a concentration range of 0 – 30 mg L^{-1} for each metal, and the samples were properly diluted when necessary.

Synthetic single- and multi-element solutions mimicking the mother solution were prepared using $NiCl_2{\cdot}6\ H_2O$, $MnCl_2{\cdot}4\ H_2O$, $CoCl_2{\cdot}6\ H_2O$, and LiCl (Sigma-Aldrich® and Fluka®, purity ≥ 99 %). Sodium hydroxide (NaOH) solutions for pH adjustment were prepared from concentrated stock solutions. A multi-element standard solution (100 mg·L^{-1} of each metal in 5 % HNO_3, CPAchem) was used for ICP-OES calibration. All solutions were prepared with deionized water (resistivity 18 MΩ cm) and class A glassware.

A 5 kg sample of pomace (seeds, pulp and deoiled flavedo post-extraction of essential oil and juice) from *Citrus Bergamia* cultivars *Femminello* and *Fantastico*, harvested between November 2021 and January 2022, was provided by *Capua 1880* (Reggio Calabria, Italy). The pomace pretreatment protocol was assessed simplifying that already reported in previous literature findings [36–38]. Briefly, aliquots of the biomass were oven-dried (2001244, J.P. Selecta, Barcelona, Spain) at t = 60 °C until constant weight was achieved (~ 48 h) with a loss of about 60 % in weight. The dried material was ground using a coffee grinder (YM-1107 Nirva, Yiwu Youma Technology, Yiwu, China) to a fine powder and treated with deionized water. In detail, 5 g of dry pomace was placed into 50 cm^3 Falcon® tubes and deionized water was added dropwise using a burette to obtain a solid-to-liquid ratio of 100 g dm^{-3}. The mixture was agitated for 1 h in an orbital shaker (PTR-35 Grant Bio, Grant Instruments, Cambridge, UK) and then centrifuged at 5000 rpm for 10 min at t = 25 °C (NEYA 16 R, Giorgio Bormac, Modena, Italy). The resulting brownish aqueous phase was separated and collected for pH measurement using a 713 pH meter equipped with a 6.0233.100 combined glass electrode (Metrohm, Herisau, Switzerland). The recovered solid was subjected to successive washing cycles adding further 50 cm^3 of deionized water, mixtures were kept undisturbed for 1 h and centrifuged again, until the difference in measured pH between two consecutive cycles was less than 0.05 pH units. The final washed solid was oven-dried at t = 60 °C until constant weight (~ 24 h) and designated as BP.

Three sets of isotherm experiments were conducted: i) with four single-component synthetic solutions (one for each metal cation), ii) with a synthetic multi-component solution containing all metal cations in concentration ratios simulating the real spent cathode leachate, and iii) with the mother solution obtained from the RJ-EtGly spent cathode.

In all cases, experiments were performed in batch mode by adding a weighed amount of BP (m ~ 0.0200 g) into Erlenmeyer flasks. A proper volume of aqueous solutions (V = 0.030 dm^3 or 0.1 dm^3) containing the target metal cation(s) (either single-component, synthetic multi-component, or real spent cathode leachate) at varying initial analyte concentrations (c_0) was then added. The flasks were covered to prevent evaporation and/or contamination and agitated in an orbital shaker at a constant temperature (25.0 ± 0.1 °C). After 24 h, namely the time required to reach thermodynamic equilibrium, the mixtures were filtered through a 0.45 μm cartridge, and the equilibrium analyte concentration in solution (c_e) was determined by ICP-OES. The complete dataset for the three sets of batch isotherm experiments is given in Table S1.

The pomace adsorption capacity towards metal cations (q_e, mmol g^{-1}) at different sorbent-to-metal ratios was calculated according to Eq. (1)

$$q_e(\text{mmol g}^{-1}) = \frac{V(\text{dm}^3) \bullet (c_0 \ (\text{mmol dm}^{-3}) - c_e(\text{mmol dm}^{-3}))}{m(\text{g})} \quad (1)$$

2.2. Characterization protocols

Raman spectra were collected with a Renishaw spectrometer (Nanonics Multiview 2000) using a 532 nm excitation wavelength. Each spectrum was acquired with a 15-second laser exposure, and measurements were recorded at three different spots on each sample to ensure reproducibility.

The positive electrode from the used battery and the RJ-EtGly powder were characterized as recovered by means of X-ray diffraction (XRD) to confirm the crystal structure and detect possible secondary phases. Diffraction patterns were obtained using a Bruker D8 Discover diffractometer equipped with an LYNXEYE XE detector and Cu Kα radiation (λ =1.54060 Å) over the 2Θ range of 10–80°.

Thermogravimetric analysis (TGA) was performed on a Netzsch TG 209 F1 instrument, with a heating rate of 5 °C min^{-1} from 30 °C to 800 °C under an oxygen atmosphere.

TOC and IC measurements of ultrapure water (blank), the leachate solution, and post-adsorption solutions were carried out with a Shimadzu TOC-5050 system based on the combustion catalytic oxidation method coupled with a Shimadzu ASI-5000A autosampler.

2.3. Calculations

The experimental adsorption equilibria data (c_e and q_e) were fitted using the well-known Freundlich (Eq. (2)) and Langmuir (Eq. (3)) isotherm models:

$$q_e = K_F \cdot c_e^{1/n} \quad (2)$$

$$q_e = \frac{q_m \cdot K_L \cdot c_e}{1 + K_L \cdot c_e} \quad (3)$$

where K_F ($dm^{3/n}\ g^{-1}\ mmol^{1-1/n}$) is the Freundlich constant or maximum adsorption capacity, q_m is the maximum adsorption capacity of the biomass (mmol g^{-1}), and K_L ($dm^3 \cdot mmol^{-1}$) is the Langmuir affinity constant.

The fitting quality was evaluated using the correlation coefficient (R^2), adjusted correlation coefficient (adj. R^2), and Root Mean Square Error (RMSE) as defined in Eqs. (4)–(6).

$$R^2 = 1 - \frac{\text{Residual sum of squares}}{\text{Total sum of squares}} = 1 - \frac{\sum_{i=1}^{N}(q_{e_i} - \widehat{q_{e_i}})}{\sum_{i=1}^{N}(q_{e_i} - \overline{q_{e_i}})} \quad (4)$$

$$\text{adj. } R^2 = 1 - \left[\frac{(1 - R^2)\cdot(N - 1)}{(N - k - 1)}\right] \quad (5)$$

$$\text{RMSE} = \sqrt{\frac{\sum_{i=1}^{N}(q_{e_i} - \widehat{q}_{e_i})^2}{N}} \quad (6)$$

where, for an isotherm experiment with N data points and k = 1 independent variables, q_{e_i}, $\widehat{q_{e_i}}$, and $\overline{q_{e_i}}$ are the i^{th} experimental, predicted (from the Freundlich or Langmuir model) and average adsorption capacity, respectively.

3. Results and discussion

3.1. Characterization of the RJ-EtGly spent cathode

Elemental concentrations in the *mother solution* determined by ICP-OES were 139 mg dm^{-3} Li, 428 mg dm^{-3} Ni, 129 mg dm^{-3} Mn, and 167 mg dm^{-3} Co. These correspond to approximate mass ratios of 1:3:1:1 and molar ratios of Li:Ni:Co:Mn ≈ 1:0.37:0.12:0.14. Roughly, 15 % of the cathode composition consisted of non-metallic components, primarily carbon.

The Raman spectrum of the RJ-EtGly powder, shown in Fig. 1, confirmed the presence of carbon black. Two broad bands were observed: the D band (~1350 cm^{-1}), associated with disordered sp^2 carbon, and the G band (~1580 cm^{-1}), characteristic of graphitic domains. These signals originate from the conductive carbon added to enhance electrode electronic conductivity, which was not removed during the powder harvesting. The spectral features are consistent with a partially disordered, high-surface-area carbon structure commonly used in battery electrodes. The size of the graphitic domains was estimated from the D-to-G band intensity ratio (I_D/I_G). After baseline subtraction, the integrated areas of the two bands yielded an I_D/I_G ratio close to 0.21. Using the relation proposed by Cancado *et al.* [39], which accounts for the excitation wavelength (λ = 532 nm), the calculated in-plane crystallite size was prudentially estimated as 92 ± 10 nm, in line with typical domain sizes reported for nanostructured graphite materials [40]. Moreover, a prominent peak was observed at ~ 590 cm^{-1}, corresponding to the A_1g vibrational mode of the layered NMC structure, associated with the symmetric stretching of oxygen in the MO_6 octahedra (M = Ni, Mn, Co) [41].

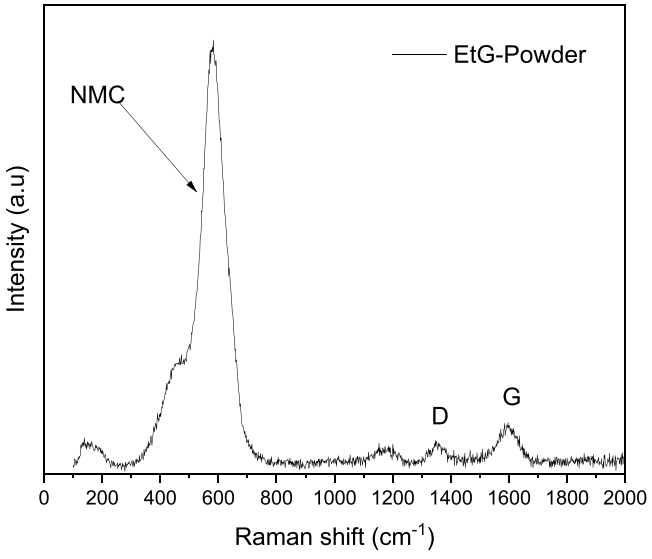

Fig. 1. Raman spectrum of the recovered RJ-EtGly powder.

The Le Bail fitting of the XRD pattern for the pristine sample electrode and the delaminated powder with ethylene glycol is presented in Fig. 2. The expected reflections of the *R3m* phase align with the peaks observed in the sample, with a slight shift being noticed. Residuals of the binder can be observed in the reflection at 26.5° for the pristine sample. Hence, this reflection disappears for the RJ-EtGly powder delaminated sample. From the refined lattice constants (α-$NaFeO_2$ structure), the value for the cell parameter of the pristine is a ≈ 2.86 Å and c ≈ 14.28 Å, and for the recovered sample is a ≈ 2.89 Å and c ≈ 14.16 Å. Besides the similarity with the rhombohedral layered (*R3m*) structure, two differences are observed: an expansion of a and a contraction of c, which can be attributed to slight changes in the Li content or cation mixing. Another difference is that in the pristine state, the clear split of the 006/102 and the 108/110 peaks, related to the crystallinity and good hexagonal structure, is lost once the material is delaminated, and could be associated with the washing steps.

3.2. Adsorption isotherm experiments of single metal solutions

The first set of experiments focused on adsorption tests using single-cation synthetic solutions. Seven solutions with increasing metal concentrations were prepared and contacted with approximately 0.020 g of BP, resulting in markedly different metal-to-site ratios. This design allowed us to explore both metal-excess and site-excess conditions, assuming a surface site density of 1.10 mmol g^{-1} for BP, as reported in the literature [36]. Full experimental details are given in Table S1. Scatter plots of the adsorption capacity (q_e, Eq. 1) *vs.* the equilibrium concentration of metal cations (c_e, experimentally determined) for the batch isotherm experiments with synthetic mono-elemental solutions are shown in Fig. 3 for Mn^{2+}, Co^{2+} and Ni^{2+}. Li^+ recovery was negligible, and the corresponding data were not reported. The adsorption capacity

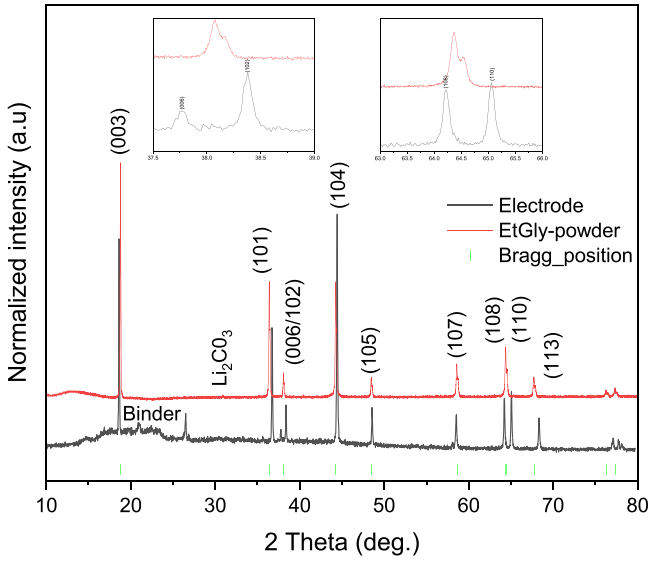

Fig. 2. Le Bail fits of the XRD patterns of electrode and RJ-EtGly powder recovered from the electrode.

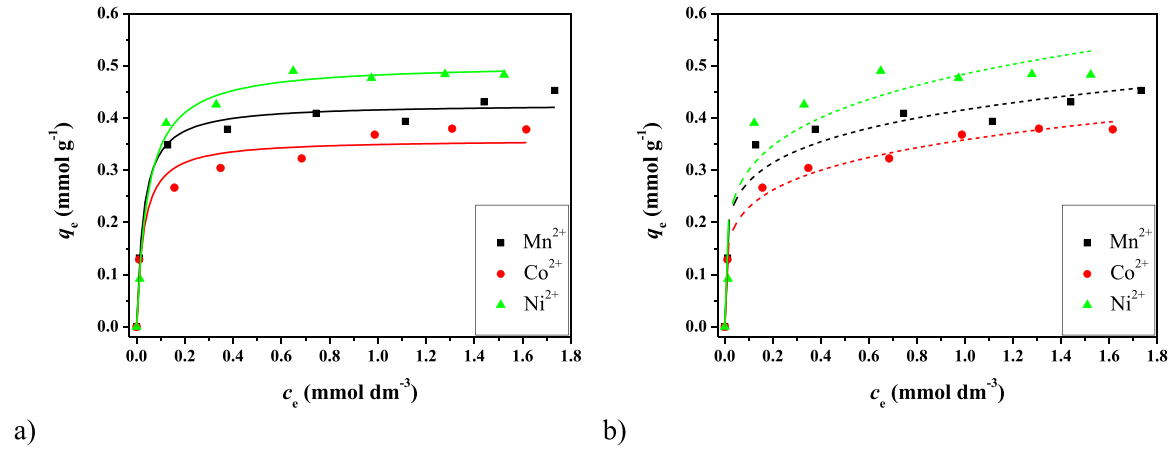

Fig. 3. Adsorption isotherms of Mn^{2+}, Co^{2+} and Ni^{2+} ions in single metal solutions on BP at pH = 5 and t = 25 °C. The experimental data were processed using the Langmuir (a) and Freundlich (b) model equations.

increased with cation concentration, reaching a plateau at ~0.4–0.6 mmol dm^{-3} , indicating that BP effectively adsorbs the divalent cations.

Experimental data for Ni^{2+}, Mn^{2+}, and Co^{2+} were successfully fitted with both Langmuir (Eq. 3, Fig. 3a) and Freundlich (Eq. 2, Fig. 3b) isotherm models. The resulting fitting parameters, including adjusted-R^2 and RMSE values, are summarized in Table 1. The Langmuir model described the experimental data for Ni^{2+} and Mn^{2+} more accurately than the Freundlich model, whereas the latter yielded a better fit for Co^{2+}. As expected for natural sorbent materials, the q_m and K_L values were comparable across the three divalent metal cations in the single-metal systems, suggesting non-specific interactions between the metal cations and BP surface functional groups. This finding is consistent with the low affinity of carboxylate groups, abundant in BP [36], towards lithium ions, thereby supporting the accuracy and reliability of the experimental results.

Minor differences were nevertheless observed among the cations. The affinity, estimated by K_L, of BP towards the three metal cations was not statistically different, whereas the maximum adsorption capacity (q_m) followed the trend: $Ni^{2+} > Mn^{2+} > Co^{2+}$. This behavior is consistent with the slightly smaller hydrated radius and higher charge density of Ni^{2+} compared to Co^{2+} and Mn^{2+} [42] factors that marginally enhance its interaction with oxygen-donor functional groups present in BP. These findings highlight the ability of BP to efficiently adsorb divalent transition-metal cations from aqueous solutions, albeit with varying efficiency.

3.3. Adsorption Isotherms of synthetic multicomponent solution

After assessing thermodynamic equilibrium behavior in single-metal systems, experiments were extended to a more realistic scenario using a synthetic multicomponent solution designed to simulate the leachate composition of spent RJ-EtGly LIBs cathodes. The synthetic multicomponent solution, prepared from chloride salts (non-primary standard reagents), was analyzed by ICP-OES, yielding 118 mg dm^{-3} Li, 454 mg dm^{-3} Ni, 116 mg dm^{-3} Mn, and 205 mg dm^{-3} Co. Diluted aliquots of this stock solution were subsequently used to prepare the adsorption batches for BP contact. Since the synthetic multicomponent solution contained four different metal cations with distinct analytical concentrations and affinities toward BP surface functional groups, careful experimental planning was required. Specifically, for each metal cation, the variation in residual concentration in solution had to be sufficiently large to be accurately quantified by ICP-OES, and the metal-to-sorbent ratio had to span conditions both below and above saturation in order to reliably estimate the Langmuir (K_L, q_m) and Freundlich (K_F) parameters. For the Langmuir model in particular, batches with cations in deficit relative to BP functional groups were essential to observe a significant variation in adsorption capacity (q_e) and, consequently, to estimate K_L. In contrast, batches with cations in excess were required to observe saturation and determine q_m (full experimental details given in Table S2). These requirements applied independently to each metal cation, making the experimental planning inherently complex. Sixteen batches were deemed sufficient for parameter estimation based on the results obtained from single-component systems (*i.e.*, affinity and maximum adsorption capacity). Nevertheless, equilibrium established in each batch containing all four cations remained challenging to interpret, as Ni^{2+}, Mn^{2+}, and Co^{2+} exhibit relatively similar affinities for the adsorption sites. However, since Ni^{2+} was present at a relatively higher concentration than Co and Mn, its interaction with adsorption sites was favored, even from a purely statistical standpoint. Scatter plots of the experimental data for Ni^{2+}, Mn^{2+} and Co^{2+} are presented in Fig. 4, with Langmuir (a) and Freundlich (b) fits; the corresponding fitting parameters are listed in Table 2. Under these conditions, BP exhibited selective adsorption, showing the highest capacity for Ni^{2+} (q_m = 0.152 mmol g^{-1}), whereas Mn^{2+} and Co^{2+} were adsorbed at similar levels (0.054 and 0.047 mmol g^{-1}, respectively). These q_m values closely followed the relative concentration ratios of the cations in the synthetic solution, suggesting that when the sorbent displays comparable affinity for multiple analytes (as indicated by the single-component results in Table 1), competitive adsorption leads to capacities proportional to analyte concentrations. In other words, in the absence of strong intrinsic selectivity, the observed q_m values result from the relative availability of the competing ions in a concentration-driven competition scenario. This supports the hypothesis that the total adsorption capacity

Table 1
Langmuir and Freundlich parameters for the adsorption of M^{2+} ions in single metal solutions on BP at pH = 5 and t = 25 °C.

Metal	q_m [a]	K_L [b]	Adj-R^2 [c]	RMSE [d]	K_F [e]	n	Adj-R^2 [c]	RMSE [d]
Mn^{2+}	0.43 ± 0.01	36 ± 7	0.986	0.018	0.42 ± 0.02	6 ± 1	0.944	0.036
Co^{2+}	0.36 ± 0.02	36 ± 14	0.951	0.028	0.36 ± 0.01	5.1 ± 0.4	0.989	0.013
Ni^{2+}	0.50 ± 0.01	22 ± 3	0.992	0.016	0.48 ± 0.02	5 ± 1	0.896	0.058

[a] in mmol g^{-1} ± std. dev.; [b] in dm^3 mmol^{-1} ± std. dev.; [c] adjusted R-squared; [d] root mean square error; [e] in dm$^{3/n}$ g^{-1} mmol$^{1-1/n}$ ± std. dev.

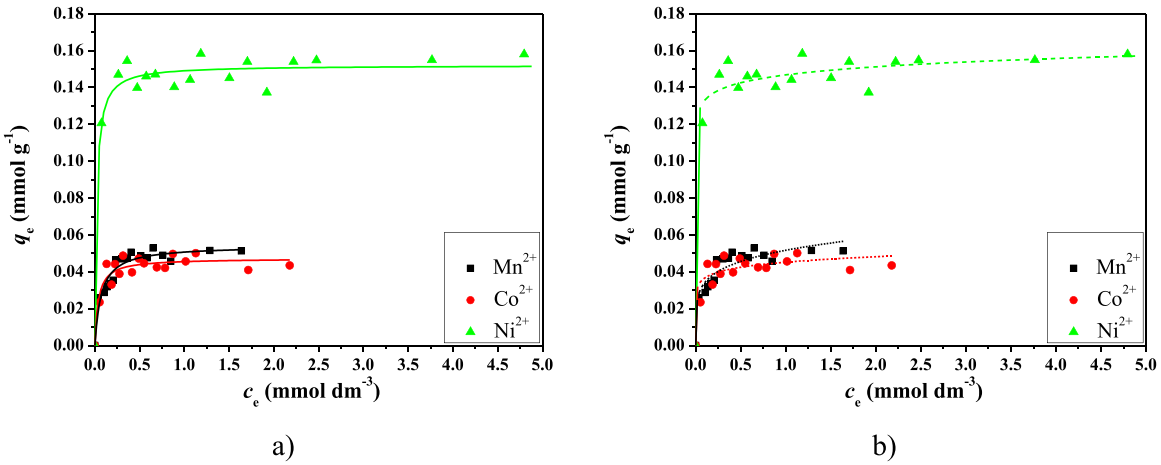

Fig. 4. Adsorption isotherms of Mn^{2+}, Co^{2+} and Ni^{2+} ions in synthetic multicomponent solution on BP at pH = 5 and t = 25 °C. The experimental data were processed using the Langmuir (a) and Freundlich (b) model equations.

Table 2
Langmuir and Freundlich parameters for the adsorption of Mn^{2+}, Co^{2+} and Ni^{2+} ions in synthetic multicomponent solution at pH= 5 and t = 25 °C.

Metal	q_m [a]	K_L [b]	Adj-R^2 [c]	RMSE [d]	K_F [e]	n	Adj-R^2 [c]	RMSE [d]
Mn^{2+}	0.054 ± 0.002	14 ± 3	0.919	0.004	0.052 ± 0.001	6 ± 1	0.891	0.004
Co^{2+}	0.047 ± 0.002	26 ± 9	0.867	0.004	0.045 ± 0.002	11 ± 4	0.799	0.005
Ni^{2+}	0.152 ± 0.002	50 ± 16	0.962	0.007	0.147 ± 0.001	23 ± 7	0.956	0.007

[a] in mmol g^{-1} ± std. dev.; [b] in dm^3 $mmol^{-1}$ ± std. dev.; [c] adjusted R-squared; [d] root mean square error; [e] in $dm^{3/n}$ g^{-1} $mmol^{1-1/n}$ ± std. dev.,

of BP in a multicomponent system can be approximated by summing the individual q_m contributions for single-metal systems.

The consistently lower q_m values observed in multicomponent solutions, compared to single-metal systems, are consistent with competitive adsorption effects. The differences in affinity trends between single and synthetic multicomponent systems may also reflect experimental limitations: despite the careful design, the dataset lacks sufficient low-concentration points, especially for Ni^{2+}, which hinders accurate estimation of K_L values in the initial isotherm region.

3.4. Adsorption Isotherms of multicomponent solution from spent RJ-EtGly cathode

For the real leachate solution, the design of the experiments followed the same approach used for the synthetic multicomponent solution, based on the concentration of the ***mother solution*** reported in 3.1. Thus, a total of sixteen batches were prepared by diluting the ***mother solution*** and contacting it with BP aliquots (full experimental details are given in Table S3). Experimental data were fitted using both the Langmuir and Freundlich isotherm model equations, with the results summarized in Table 3. The scatter plot of adsorption capacity (q_e) versus equilibrium concentration (c_e) is shown in Fig. 5, with Langmuir (a) and Freundlich (b) fits. As in the synthetic system, the Langmuir model provided a better description of the equilibrium data.

BP demonstrated relevant adsorption capacity for the target metal ions, with Ni^{2+} showing the highest value (q_m = 0.488 mmol g^{-1}). This capacity was approximately three to four times higher than that observed for Co^{2+} and Mn^{2+}, consistent with the selectivity trends obtained in the synthetic multicomponent solution (see Fig. 4).

Here it is worth to briefly discuss on the operative details of the adsorption equilibria since the outcome of the above experiments refers to a real spent NMC622cathodic material. In this sense, a crucial point relies on the operative pH whose choice (at pH = 5; see Experimental Section) was supported by a combined evaluation of both the acid–base properties of BP and the metal species in solution. Our previous characterisation studies have shown that BP exhibits a point of zero charge (PZC) of 3.46 and that carboxylic groups constitute the predominant active sites responsible for metal ions binding. Potentiometric titrations allowed the determination of the protonation constant of the -COOH groups (log K^H = 3.65 ± 0.01) indicating that at pH ≥ 4 these functionalities are largely deprotonated and therefore available for interaction with divalent cations [36]. Furthermore, previous adsorption experiments of Nd^{3+} and Dy^{3+} onto BP, conducted at pH 3, 4 and 5, corroborate this interpretation, showing that the adsorption capacity of BP remains essentially unchanged between pH 4 and 5, whereas a marked decrease at pH 3 results from protonation of the carboxylic groups and competition between the H^+ and metal cations for the active sites [38]. Considering metal ions speciation, as already mentioned in the Experimental Section, Mn^{2+}, Ni^{2+} and Co^{2+} are known to remain as soluble aquo ions at pH < 6. Altogether, these considerations define a broad and reliable operating window between pH 4 and 6, which is compatible with industrial conditions where maintaining a strictly controlled pH is not always feasible.

The q_m values obtained for the real leachate were significantly higher than those measured for the synthetic multicomponent solution, suggesting that specific chemical and physical factors intrinsic to the

Table 3
Langmuir and Freundlich parameters for the adsorption of M^{2+} ions in multicomponent solution from spent NMC cathode at pH= 5 and t = 25 °C.

Metal	q_m [a]	K_L [b]	Adj- R^2 [c]	RMSE [d]	K_F [e]	n	Adj-R^2 [c]	RMSE [d]
Mn^{2+}	0.145 ± 0.009	6 ± 1	0.907	0.011	0.122 ± 0.006	3.6 ± 0.6	0.824	0.015
Co^{2+}	0.096 ± 0.003	16 ± 2	0.960	0.005	0.099 ± 0.003	4.2 ± 0.4	0.947	0.006
Ni^{2+}	0.488 ± 0.001	2.5 ± 2	0.990	0.012	0.329 ± 0.008	2.6 ± 0.2	0.954	0.025

[a] in mmol g^{-1} ± std. dev.; [b] in dm^3 $mmol^{-1}$ ± std. dev.; [c] adjusted R-squared; [d] root mean square error; [e] in $dm^{3/n}$ g^{-1} $mmol^{1-1/n}$ ± std. dev.

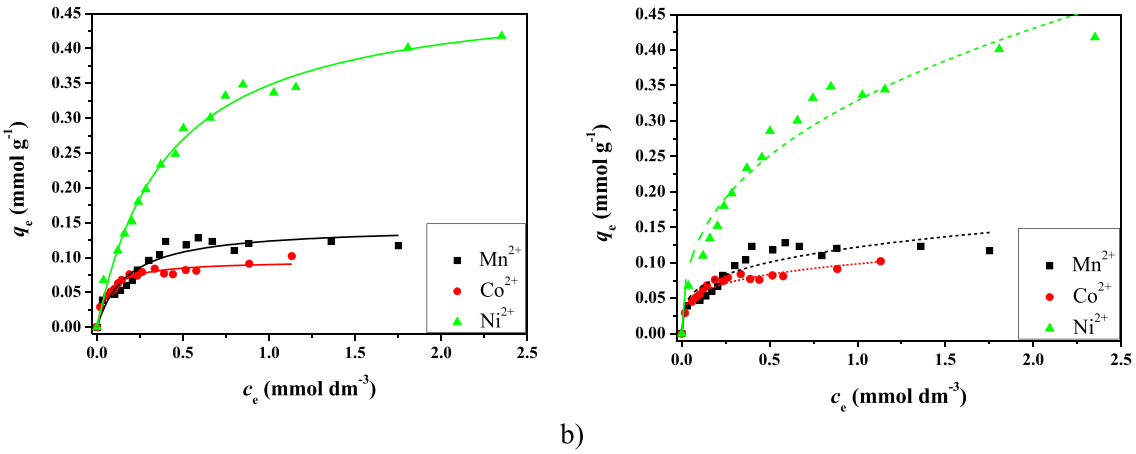

Fig. 5. Adsorption isotherms of Mn^{2+}, Co^{2+} and Ni^{2+} ions in multicomponent solution from spent NMC cathode on BP at pH= 5 and t = 25 °C. The experimental data were processed using the Langmuir (a) and Freundlich (b) model equations.

leachate matrix may have contributed to the enhanced adsorption performance. This unexpected result prompted a series of considerations aimed at identifying matrix-specific factors that could plausibly account for the observed discrepancy.

First, the potential interference of chloride ions in the synthetic multicomponent solution, since the preparation involved chloride salts. Chloride can combine with metal cations to form species such as $MnCl^+$, which, due to their reduced effective charge (1^+ *vs.* 2^+), are expected to interact less effectively with the active sites of BP. However, speciation calculations performed with PyES software [43] based on the analytical concentrations of metal cations and chloride as well as equilibrium constants taken from the JESS database [44], indicate that such complexes represent less than 5–6 % of the total dissolved metal species. Thus, most cations remain as aquo-ions, and chloride complexation alone cannot account for the enhanced q_m values observed in the real leachate.

Second, the possible contribution of organic substances generated during the leaching process of the spent cathode. These could, in principle, promote metal precipitation through oxidation of carbonaceous components in the cathode during treatment with an HNO_3/H_2O_2 mixture. However, TOC and IC analyses of ultrapure water (as blank), the leachate solution, and post-adsorption solutions revealed negligible concentrations of dissolved organic matter (TOC ~5 mg dm^{-3}, IC ~ 0.1 mg dm^{-3}), not significantly different from the blank. This evidence suggests that organic species do not play a significant role in the increased adsorption performance.

Another crucial aspect is the difference in ionic strength between the two systems. The real leachate exhibited an ionic strength of about 0.175 mol dm^{-3}, nearly three times higher than that of the synthetic solution (0.06 mol dm^{-3}), mainly due to the addition of HNO_3 for the leaching and to NaOH for acid neutralization. This increase in ionic strength may lead to a) a variation of the affinity between metal cations and the functional groups (-COOH and -OH) on the biosorbent surface and, more generally, modify the chemical speciation of the solution; b) a compression of the electrical double layer [45,46], which may facilitate the interaction of metal cations with the surface-active sites, thus contributing to the increase in adsorption capacity. Again, such effects do not fully explain the enhanced adsorption capacity.

Given these elements, our attention shifted from the solution composition to the solid fraction originating from the spent cathode.

A plausible explanation for the enhanced adsorption observed in the real leachate involves the presence of carbonaceous particles originating from the spent cathode (see 3.1), which are absent in the synthetic multicomponent solution. Raman spectrum collected from the RJ-EtGly precursor material consistently revealed graphitic domains with characteristic dimensions of ~90 nm. Particles of this size are well below the 0.45 μm cutoff of the membrane filters used during the preparation of the leachate solution prior to adsorption, and may therefore remain suspended during the sorption experiment. Under such conditions, these nanoscale carbon particles could participate in metal removal through co-adsorption or microprecipitation at the carbon–solution interface. Similar colloidal destabilization processes have been reported in the literature [47], particularly in systems subjected to strong electrolyte addition, such as those occurring during leaching and subsequent pH adjustment, which are known to reduce electrostatic repulsion within the electrical double layer.

The plausibility of carbonaceous colloids in hydrometallurgical leachates is supported by Wu et al. [28], who showed that LIB leaching generates carbon-rich residues originating from graphite and organic reductants, with substantial carbon content persisting after centrifugation and 0.45 μm filtration. Since our leaching conditions are comparable, these findings reinforce the likelihood that sub-micron carbonaceous particles remain in solution after filtration in our system as well.

Nonetheless, the proposed mechanism remains a working hypothesis. Although supported by Raman evidence and of graphitic phases in the parent material and particle-size considerations relative to the filtration threshold and consistent with other literature study [28], the actual presence and behavior of such colloidal carbon particles in the leachate were not directly measured in this study. A dedicated microstructural investigation would require further verification by means of dedicated instrumentation (*e.g.*, TEM, DLS).

Taken together, these matrix-specific effects mitigate the competitive suppression observed in the synthetic mixture and allow Ni^{2+} to retain an adsorption capacity close to that measured in the single-component system, while Co^{2+} and Mn^{2+} remain more strongly affected by competition. This explains both the unusually high q_m of Ni^{2+} and the intermediate q_m values of Co^{2+} and Mn^{2+} observed in the real leachate.

Further insights into the adsorption process come from thermogravimetric analysis (TGA), in Fig. 6. The residual mass of RJ-EtGly sample and derivative thermogravimetry (DTG) profiles are shown in the top left panel of Fig. 6, whereas the profile interpretation in terms of temperature range, % of mass loss, and chemical processes involved is given in Table 4. In detail, an initial mass loss between 180–333 °C (3.15 %) was attributed to the evaporation or decomposition of residual ethylene glycol retained from the delamination process [48]. Two subsequent mass losses were observed between 333–440 °C (binder, 2.5 %) and 440–563 °C (conductive carbon, 2.6 %), in agreement with literature data [49].

The fresh pomace (Fig. 6, top right panel) displayed a broad thermal degradation profile, with a total mass loss of approximately 30 %

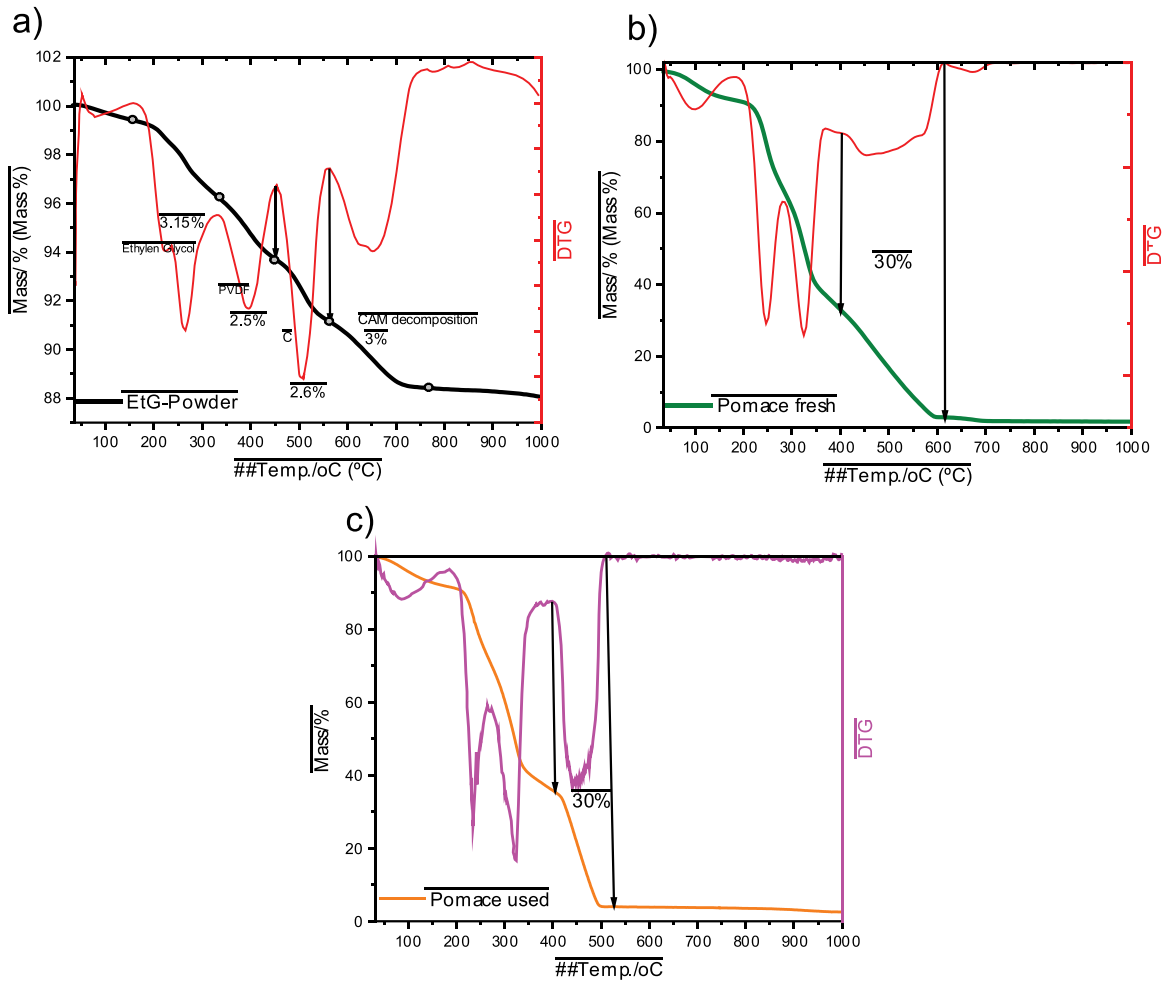

Fig. 6. Thermogravimetric analysis of RJ-EtGly powder (top left, a), fresh pomace (top right, b), and pomace used (down, c) for cation sorption from the spent cathode leachate solution.

Table 4
Summary of the processes observed on the RJ-EtGly cathode.

Temperature Range (°C)	Mass Loss (%)	Process involved
180–333	3.15	Evaporation of residual Ethylene Glycol
333–440	2.5	Decomposition of PVDF binder
440–563	2.6	Oxidation of conductive carbon additives

between 400 °C and 620 °C [36], whereas the used pomace (Fig. 6, down panel) showed a similar total loss (~30 %) but within a narrower temperature range (400–520 °C) with a more pronounced DTG peak. This behavior suggests an accelerated thermal degradation, likely due to the catalytic effect of transition metals (Ni^{2+}, Co^{2+}, Mn^{2+}) adsorbed onto the pomace surface after the recovery process, as these metals are known to reduce the activation energy of combustion reactions. These observations confirm that the presence of adsorbed transition metals modifies the oxidative degradation pathway of BP, accelerating its combustion relative to the pristine biomass. It should also be noted that TGA/DTG experiment was conducted under an oxidative atmosphere in order to assess the decomposition behavior of BP and evaluate the catalytic influences of transition metal cations on the oxidation kinetics of the material. Although this work does not aim to develop or optimize post-adsorption metal recovery routes, it is important to note that phase and morphology analysis of the ash obtained after controlled oxygen calcination could provide valuable insight into metal occurrence states, particularly for studies focused on downstream regeneration or oxide precursor production. These aspects will be explored in future work dedicated to the recovery of adsorbed metals after biosorbent utilization. From this overall analysis, it emerges that the differences in q_m values between the synthetic multicomponent solution and the spent cathode leachate cannot be attributed to a single factor. Instead, they result from the combined effect of multiple synergistic contributions. The partial interference given by chloride ions, the presence of nano-sized graphitic carbon in the filtered leachate, and increased ionic strength represent the main triggers. In contrast, the potential effects of dissolved organic substances derived from the oxidation of carbonaceous particles upon the leaching can be excluded, as they are not supported by the experimental data.

3.5. Selectivity analysis

To better quantify the selectivity of BP toward Ni^{2+}, Co^{2+} and Mn^{2+} in multicomponent systems, distribution coefficients (K_d) were calculated according to Park et al. [50] at three representative regions of the isotherms - low, intermediate and high equilibrium concentrations - corresponding respectively to the initial high-affinity domain, an intermediate loading range, and conditions approaching sorbent saturation (Table S4).

In the synthetic multicomponent system, K_d values at low equilibrium concentrations (Batch 1) follow the trend $Ni^{2+} > Mn^{2+} > Co^{2+}$. However, at intermediate and high loadings (Batches 8 and 16), the K_d

values converge to similar magnitudes. This behavior confirms that BP does not exhibit strong intrinsic selectivity among the three cations, and that the larger q_m observed for Ni^{2+} in this system primarily reflects its higher initial concentration rather than a marked chemical preference of the sorbent.

In the real leachate, K_d values remain consistently higher for Ni^{2+} than for Co^{2+} and Mn^{2+} across all examined concentrations, with the difference becoming more pronounced at intermediate and high loadings. This indicates a moderate preference of BP for Ni^{2+} under realistic conditions, likely arising from smaller hydrated radius and higher charge density of Ni^{2+} compared to Co^{2+} and Mn^{2+} (see 3.2), and matrix-specific effects (*i.e.*, increased ionic strength and presence of carbonaceous colloids). Overall, the distribution-coefficient analysis corroborates the view that BP can act as an effective polishing sorbent, with a modest but measurable selectivity towards Ni^{2+} with respect to Co^{2+} and Mn^{2+} in multicomponent LIB leachates.

3.6. Environmental and economic assessment

To evaluate alternative strategies aimed at improving the sustainability of lithium-ion battery (LIB) recycling, it is essential to integrate a detailed analysis of production processes with a comprehensive assessment of environmental impacts [51]. The Life Cycle Inventory (LCI) provides a quantitative overview of the material and energy inputs required to produce 1 kg of BP. The estimated values of energy demand and global warming potential (GWP), reported in a previous study on rare earth element recovery [38], offer valuable insights into the potential environmental impacts of each process stage and help identify key "hotspots" and opportunities for process optimization. In this work, the environmental performance and production costs of BP are evaluated by distinguishing two configurations, laboratory scale (LS) and prospective industrial scale (IS), differing exclusively in the drying stage, which is the most energy-intensive step of the biosorbent preparation process. All other operations (washing, centrifugation, grinding, etc.) are modelled under laboratory scale conditions. In the LS scenario, drying is carried out using a low-efficiency laboratory oven operated in two consecutive cycles, resulting in a total energy demand of 13.48 kWh per kg of dried BP (full details are given in supporting information). This value reflects the long residence times and the absence of heat-recovery features that characterize laboratory equipment. In the prospective industrial scale (IS) scenario, only the dehydration stage is optimized by assuming the adoption of a high-efficiency belt dryer, a technology widely employed for agro-industrial biomasses, which reduces the electricity consumption to 2.9 kWh kg^{-1} [52]. Thus, even when industrial optimization is applied solely to the drying phase, the energy demand decreases by approximately 78 % relative to the LS configuration, highlighting the relevance of drying technologies equipped with partial heat-recovery systems. Accordingly, the analysis of the data presented in Table 5 indicates that drying is the most energy-intensive stage of the process, contributing predominantly to both overall energy consumption and production costs.

Table 5
Life Cycle Inventory (LCI) to produce 1 kg of BP.

Material and cost input	Unit	Lab scale (LS)	Industrial scale (IS)
Bergamot pomace mass	kg	4.16	4.16
Drying electricity consumption[a]	kWh	13.48	2.9
Grinding electricity consumption[a]	kWh	0.225	0.225
Shaking electricity consumption[a]	kWh	0.272	0.272
Centrifuge electricity consumption[a]	kWh	1.9	1.9
Electricity cost[b]	€ kWh^{-1}	0.3	0.3
Deionized water	dm^3	166.66	166.66
Water cost[c]	€ dm^{-3}	0.06	0.06
Total	€ kg^{-1}	14.76[d]	11.60[d]

[a] Energy consumed in each process step; [b] average electricity price [53]; [c] average price of deionized water considering the system used in the lab; [d] the full equation used for this estimation is reported in the supporting information.

The consumption of deionized water remains constant between the two cases (166.66 dm^3 per kg of BP), representing a non-negligible contribution to operating costs, particularly at laboratory scale. However, its environmental impact is secondary compared with energy consumed during drying. To evaluate the potential of BP as a complementary material within hydrometallurgical recycling flows, production costs and adsorption capacities were compared with those of ion-exchange resins and activated carbons, commonly employed for metal removal from aqueous solutions. Although not intended to replace existing hydrometallurgical technologies, BP can act as a secondary recovery step for residual metal cations remaining in leachates after primary extraction. The comparison with literature data confirms that the adsorption capacities (q_m) of BP for Ni^{2+} (0.488 mmol g^{-1}), Co^{2+} (0.096 mmol g^{-1}), and Mn^{2+} (0.145 mmol g^{-1}) fall within the typical ranges reported for ion-exchange resins (Ni^{2+}: 0.400–0.550 mmol g^{-1}, Co^{2+}: 0.100–0.180 mmol g^{-1}, Mn^{2+}: 0.150–0.200 mmol g^{-1}) [20] and activated carbons (Ni^{2+}: 0.200–0.350 mmol g^{-1}, Co^{2+}: 0.050–0.100 mmol g^{-1}, Mn^{2+}: 0.100–0.150 mmol g^{-1}) [54]. To contextualize the performance of BP, Table 6 provides a quantitative comparison between the maximum adsorption capacities (q_m, mmol g^{-1}) obtained in this study and those reported for conventional biosorbents widely described in the literature [30,55–62]. The available values exhibit considerable variability: for example, ordered mesoporous carbons (PCK) show q_m values for Co^{2+} of 0.027 mmol g^{-1} [61], while dolomite reaches 0.047 mmol g^{-1} [56] and microporous F-400 activated carbons achieve 0.051 mmol g^{-1} [57]. Highly selective sorbents such as lithium ion-sieves display extremely low capacities for Co^{2+} (0.00136 mmol g^{-1}) and Ni^{2+} (0.00511 mmol g^{-1}) [62], confirming that their structure is optimized for Li^+ rather than divalent cations. Conversely, engineered materials such as activated mesoporous carbons reach very high adsorption capacities up to 0.3868 mmol g^{-1} for Co^{2+}, 0.4124 mmol g^{-1} for Ni^{2+} and 0.3822 mmol g^{-1} for Mn^{2+} [30]. Some activated carbons modified with metal oxides can also reach values of q_m = 0.5462 mmol g^{-1} for Mn^{2+} [60], whereas traditional activated carbons derived from agricultural wastes show more modest capacities, such as q_m = 0.0835 mmol g^{-1} for Ni^{2+} [58]. The q_m values obtained in this study for BP fall well within the range of conventional materials. In

Table 6
Literature values of maximum adsorption capacity (q_m, mmol g^{-1}) for Co^{2+}, Ni^{2+} and Mn^{2+} on a variety of conventional adsorbents.

Sorbent material	Sorbed metal cation	q_m (mmol g^{-1})	Ref.
Ordered mesoporous carbon (PCK)	Co^{2+}	0.0272	[61]
Dolomite	Co^{2+}	0.0475	[56]
Microporous F-400 activated carbon	Co^{2+}	0.0509	[57]
Lithium ion-sieve adsorbent	Co^{2+}	0.0014	[62]
Physicochemically activated mesoporous carbon	Co^{2+}	0.3868	[30]
Activated carbon from almond husk	Ni^{2+}	0.0835	[58]
Acid-Treated Activated Carbon	Ni^{2+}	0.0988	[55]
Lithium ion-sieve adsorbent	Ni^{2+}	0.0051	[62]
Physicochemically activated mesoporous carbon	Ni^{2+}	0.4124	[30]
Activated carbon from Birbira leaves	Mn^{2+}	0.0619	[59]
Iron oxide modified activated carbon	Mn^{2+}	0.5462	[60]
Acid-Treated Activated Carbon	Mn^{2+}	0.0273	[55]
Bergamot pomace (BP)	Ni^{2+}	0.488	This work
Bergamot pomace (BP)	Co^{2+}	0.096	This work
Bergamot pomace (BP)	Mn^{2+}	0.145	This work

single-metal systems, BP shows q_m values of 0.50 mmol g^{-1} for Ni^{2+}, 0.36 mmol g^{-1} for Co^{2+} and 0.43 mmol g^{-1} for Mn^{2+}; in the real leachate, the capacities reach 0.49 mmol g^{-1} (Ni^{2+}), 0.10 mmol g^{-1} (Co^{2+}) and 0.15 mmol g^{-1} (Mn^{2+}). Notably, the capacity obtained for Ni^{2+} in the real leachate is comparable to that of advanced mesoporous carbons, while the value for Mn^{2+} exceeds several unmodified activated carbons reported in the literature.

Given the comparable adsorption capacities of BP, it is reasonable to make a direct comparison in terms of production costs and global warming potential (GWP). In the industrial scale (IS) scenario, the production cost of BP (11.60 € kg^{-1}) is competitive with resins (5–20 € kg^{-1}) [20] and activated carbons (3–10 € kg^{-1}) [54], while its environmental impact, expressed as GWP, is significantly lower, being 0.63 kg CO_2 eq kg^{-1} for BP, 3–10 kg CO_2 eq kg^{-1} for resins and 5–12 kg CO_2 eq kg^{-1} for activated carbons. These findings position BP as a low-impact, cost-effective biosorbent. Its integration into hydrometallurgical LIBs recycling workflows could enhance metal recovery efficiency and improve overall process sustainability.

4. Conclusions

The results of this study provide a proof-of-concept for the use of BP as a platform material for the recovery of valuable metal cations from spent LIBs cathodes. The adsorption of valuable metals onto BP can be exploited within a pH operational window between 4 and 6, fully compatible with industrial conditions where precise pH control is often difficult to maintain. The sorption capacity was measured on a real acid leachate solution was approximately 0.7 mmol g^{-1} as sum of the contributions from Ni^{2+}, Mn^{2+}, and Co^{2+}, whereas Li^{+} was not recovered.

Importantly, BP demonstrated strong adsorption performance even in diluted solutions (< 30 mg dm^{-3}), suggesting that its industrial application could be particularly effective as a secondary recovery step. An additional aspect of practical relevance concerns the reusability of BP. Although regeneration tests with Ni^{2+}, Co^{2+} and Mn^{2+} are currently underway and therefore not included in the present study, the potential of BP to withstand repeated adsorption/desorption cycles has already been demonstrated in our previous work on rare earth element recovery [38], where cations were desorbed using HNO_3 and BP underwent four consecutive adsorption/desorption cycles, exhibiting excellent operational stability, with a loss of efficiency of ~ 9 % between the first and fourth cycle. Although validation with NMC-derived transition metals is still underway, the previously observed behaviour strongly suggests that BP can support multi-cycle operation also in Ni^{2+}, Co^{2+} and Mn^{2+} recovery processes.

The use of waste biomass as an adsorbent platform for metal ions not only enables their concentration but also represents a valorization pathway for an otherwise low-value material. Subsequent recovery strategies may include selective desorption with tailored solvents, thermal degradation as suggested by TG/DTA analyses, or enzymatic digestion. These approaches open perspectives for sustainable and potentially selective recovery of metals, in line with circular economy principles. We want to highlight that the present work focuses on establishing the adsorption thermodynamic of BP under controlled conditions. Although the real leachate used here reflects the chemical composition of hydrometallurgically processed NMC622 electrodes, future studies will assess BP performance in more complex matrices, including full black-mass leachates and solutions containing competing ions such as Al^{3+}, Cu^{2+} and F^{-} originating from current collectors and electrolyte degradation products. The whole of the findings highlights the potential of BP as a sustainable and cost-effective biosorbent for integration into hydrometallurgical LIBs recycling workflows, offering a complementary step to recover residual metal cations while reducing energy demand and environmental impact on a larger scale. BP is proposed as a modular secondary recovery unit designed to target the residual metal losses typically observed after electrodeposition and polishing stages. In hydrometallurgical LIB-recycling flowsheets, these downstream operations commonly exhibit cumulative cation losses of approximately 10 %; by integrating BP as an additional polishing and recovery unit, such losses may be reduced, thereby improving the overall metal yield without altering the primary leaching-purification-electrodeposition sequence.

CRediT authorship contribution statement

Roberto Di Pietro: Writing – original draft, Investigation, Formal analysis. **Stiven López Guzmán:** Writing – review & editing, Methodology, Investigation, Formal analysis. **Emilie Bekaert:** Visualization, Validation, Resources, Conceptualization. **Nicola Muratore:** Writing – review & editing, Software, Methodology, Formal analysis. **Emanuele Gucciardi:** Supervision, Project administration, Methodology, Data curation. **Salvatore Cataldo:** Validation, Resources, Investigation, Formal analysis. **Alberto Pettignano:** Resources, Project administration, Funding acquisition, Conceptualization. **Paola Cardiano:** Writing – review & editing, Writing – original draft, Supervision, Funding acquisition, Conceptualization. **Gabriele Lando:** Writing – review & editing, Writing – original draft, Project administration, Funding acquisition, Data curation, Conceptualization. **Salvatore Giovanni Michele Raccuia:** Writing – original draft, Methodology, Investigation, Formal analysis. **Davide Lascari:** Writing – original draft, Methodology, Investigation, Formal analysis.

Funding

This work was supported by Next Generation EU, Missione 4, Componente 1, CUP J53D23007540006—PRIN_2022HYH95P.

Declaration of Competing Interest

The authors declare that they have no known competing financial interests or personal relationships that could have appeared to influence the work reported in this paper.

Appendix A. Supporting information

Supplementary data associated with this article can be found in the online version at doi:10.1016/j.jece.2025.120907.

Data availability

Data will be made available on request.

References

[1] H. Li, S. Xing, Y. Liu, F. Li, H. Guo, G. Kuang, Recovery of lithium, iron, and phosphorus from spent $LiFePO_4$ batteries using stoichiometric sulfuric acid leaching system, ACS Sust. Chem. Eng. 5 (2017) 8017–8024.
[2] D.H.S. Tan, P. Xu, Z. Chen, Enabling sustainable critical materials for battery storage through efficient recycling and improved design: a perspective, MRS Energy Sustain 7 (2020).
[3] X. Wang, G. Gaustad, C.W. Babbitt, K. Richa, Economies of scale for future lithium-ion battery recycling infrastructure, Resour. Conserv. Recy. 83 (2014) 53–62.
[4] X.L. Li, X.N. Zhu, X.G. Li, X.T. Zhao, G.L. Wei, W.H. Gao, C.C. Nie, S. Yan, L.H. Ge, Z.Y. Wang, Recent advances in the extraction of critical metals from spent lithium-ion batteries: Challenges and solutions- a review, Sep. Purif. Technol. (2025) 376.
[5] G. Zang, J. Zhang, S. Xu, Y. Xing, Techno-economic analysis of cathode material production using flame-assisted spray pyrolysis, Energy 218 (2021).
[6] W. Mrozik, M.A. Rajaeifar, O. Heidrich, P. Christensen, Environmental impacts, pollution sources and pathways of spent lithium-ion batteries, Ener. Environ. Sci. 14 (2021) 6099–6121.
[7] E. Fan, L. Li, Z. Wang, J. Lin, Y. Huang, Y. Yao, R. Chen, F. Wu, Sustainable recycling technology for Li-ion batteries and beyond: challenges and future prospects, Chem. Rev. 120 (2020) 7020–7063.
[8] EU, Regulation (EU) 2023/1542 of the european parliament and of the council of 12 July 2023 concerning batteries and waste batteries, amending Directive 2008/98/EC and Regulation (EU) 2019/1020 and repealing Directive 2006/66/EC. The european parliament and the council of the european union, Official Journal of the European Union, Strasbourg, 2023.

[9] E. Mossali, N. Picone, L. Gentilini, O. Rodriguez, J.M. Perez, M. Colledani, Lithium-ion batteries towards circular economy: a literature review of opportunities and issues of recycling treatments, J. Environ. Manag. 264 (2020) 110500.
[10] M. Kaya, State-of-the-art lithium-ion battery recycling technologies, Circ. Econ. 1 (2022).
[11] L. Yun, D. Linh, L. Shui, X. Peng, A. Garg, M.L.P. Le, S. Asghari, J. Sandoval, Metallurgical and mechanical methods for recycling of lithium-ion battery pack for electric vehicles, Resour. Conserv. Recy. 136 (2018) 198–208.
[12] M. Guo, X. Xi, D. Zhang, H. Yang, F. Bi, Y. Hu, Z. Nie, K. Xu, Green and efficient method for recycling valuable metals from scrapped lithium cobalt oxide cathode materials, IOP Conf. Ser. Earth Environ. Sci. 474 (2020).
[13] K.B. Gebeyehu, L. Chen, L. Fan, Y. Chao, W. Zhu, Recovery of high-value metals from the cathode of spent lithium-ion batteries via acid leaching: a review, J. Environ. Chem. Eng. (2025) 13.
[14] K. Charzewska, J. Adamek, F. Kateusz, J. Piątek, W. Zając, Levulinic acid as a sustainable and selective leaching agent for hydrometallurgical recycling of commercial Li-ion batteries: towards greener critical metal recovery, Sep. Purif. Technol. (2026) 380.
[15] L. Gaines, Q. Dai, J.T. Vaughey, S. Gillard, Direct recycling R&D at the ReCell center, Recycling 6 (2021).
[16] L. Schlott, M. Gutsch, J. Leker, Cost modelling and key drivers in lithium-ion battery recycling, Nat. Rev. Clean. Technol. 1 (2025) 656–670.
[17] M.L. Machala, X. Chen, S.P. Bunke, G. Forbes, A. Yegizbay, J.A. de Chalendar, I. L. Azevedo, S. Benson, W.A. Tarpeh, Life cycle comparison of industrial-scale lithium-ion battery recycling and mining supply chains, Nat. Commun. 16 (2025) 988.
[18] V. Gupta, M. Appleberry, W. Li, Z. Chen, Direct recycling industrialization of Li-ion batteries: The pre-processing barricade, Energy 2 (2024).
[19] B. Wang, J. Lan, C. Bo, B. Gong, J. Ou, Adsorption of heavy metal onto biomass-derived activated carbon: review, RSC Adv. 13 (2023) 4275–4302.
[20] Y. Wu, J. Cai, X. Tang, S. Wang, M. Fang, S. Yao, J. Zhang, Efficient and selective recovery of lithium from spent lithium-ion batteries by biomass single-component regulated pyrolysis with synergistic water leaching approach, J. Env. Chem. Eng. 13 (2025).
[21] H. Jungi, A.A. Virani, S. Podder, H. Girase, J. Mitra, Sustainable combination of waste with waste: utilization of biomass to recover critical metals from spent lithium ion batteries, Batter. Supercaps 8 (2024).
[22] N. Muratore, D. Lascari, S. Cataldo, S.G.M. Raccuia, G. Lando, P. Lo Meo, V. Chiodo, S. Maisano, F. Urbani, A. Pettignano, Recovery of rare earth elements by adsorption on biochar of dead Posidonia oceanica leaves, J. Rare Earths (2024) (in press).
[23] D. Lascari, P.Lo Meo, G. Geraci, R.Lo Brutto, S.G.M. Raccuia, N. Muratore, S. Cataldo, G. Lando, E. Madonia, M. Tolazzi, A. Melchior, A. Pettignano, Insight into the adsorption of Pb^{2+} ions onto Opuntia ficus indica cladodes, J. Env. Chem. Eng. 13 (2025).
[24] K. Gupta, P. Joshi, R. Gusain, O.P. Khatri, Recent advances in adsorptive removal of heavy metal and metalloid ions by metal oxide-based nanomaterials, Coord. Chem. Rev. 445 (2021).
[25] K.L. Ong, G. Kaur, N. Pensupa, K. Uisan, C.S.K. Lin, Trends in food waste valorization for the production of chemicals, materials and fuels: case study South and Southeast Asia, Bioresour. Technol. 248 (2018) 100–112.
[26] A. Othmani, S. Magdouli, P. Senthil Kumar, A. Kapoor, P.V. Chellam, O. Gokkus, Agricultural waste materials for adsorptive removal of phenols, chromium (VI) and cadmium (II) from wastewater: a review, Environ. Res. 204 (2022) 111916.
[27] J. Sulejmanovic, E. Skopak, E. Sehovic, A. Karadza, A. Zahirovic, N. Smjecanin, O. Mahmutovic, S. Ansar, F. Sher, Surface engineered functional biomaterials for hazardous pollutants removal from aqueous environment, Chemosphere 336 (2023) 139205.
[28] Z. Wu, T. Soh, J.J. Chan, S. Meng, D. Meyer, M. Srinivasan, C.Y. Tay, Repurposing of fruit peel waste as a green reductant for recycling of spent lithium-ion batteries, Environ. Sci. Technol. 54 (2020) 9681–9692.
[29] J.Jegan Roy, E.J.J. Tang, B. Cao, M. Srinivasan, Metal extraction from commercial black mass of spent lithium-ion batteries using food-waste-derived lixiviants through a biological process, ACS Sust. Chem. Eng. 12 (2024) 16564–16576.
[30] N. Conte, J.M. Gómez, Improving the sorption properties of mesoporous carbons for the removal of cobalt, nickel and manganese from spent lithium-ion batteries effluent, Sep. Purif. Technol. 328 (2024).
[31] T. Wesselborg, S. Asumalahti, S. Virolainen, T. Sainio, Design of a continuous ion exchange process in battery metals recycling: from single column experiments towards a simulated moving bed configuration, Hydrometallurgy (2024) 228.
[32] K. Gu, W. Xia, J. Zhou, W. Qin, J. Han, From waste to wealth: novel approach for recovery of metals from spent lithium-ion batteries using biological waste, ACS Sus. Chem. Eng. 11 (2023) 13606–13615.
[33] E.G. Okonkwo, G. Wheatley, Y. Liu, Y. He, Metal recovery from spent lithium-ion batteries cathode materials: comparative study of sugar-based reductants, J. Haz. Mat. Lett. 5 (2024) 100104.
[34] C. Simanjuntak, S. Perangin-angin, A. Daulay, S.A. Amaturrahim, I.R. Saragi, D. Hussain, A. Sinuraya, Facile synthesis of nano-Si/graphite composites from rice husk for high performance lithium-ion battery anodes, Case Stud. Chem. Environ. Eng. 11 (2025) 101038.
[35] S. Suri, A. Singh, P.K. Nema, Current applications of citrus fruit processing waste: a scientific outlook, Appl. Food Res. 2 (2022).
[36] S.G.M. Raccuia, E. Zanda, C. Bretti, M. Formica, E. Macedi, A. Melchior, M. Tolazzi, M. Sanadar, D. Lascari, G. De Luca, A. Irto, C. De Stefano, P. Cardiano, G. Lando, Multi-analytical approach for the acid-base, thermal and surface properties assessment of waste biomasses, Molecules 29 (2024).
[37] A. Irto, S.G.M. Raccuia, G. Lando, C. De Stefano, K. Arena, T.M.G. Salerno, A. Pettignano, F. Cacciola, L. Mondello, P. Cardiano, Valorization of citrus waste for circular economy: a case study on bergamot pomace as sorbent for Cd^{2+} removal and source of added value compounds, Microchem. J. (2023) 193.
[38] S.G.M. Raccuia, E. Zanda, C. Bretti, M. Formica, E. Macedi, A. Melchior, M. Tolazzi, A. Pettignano, N. Muratore, D. Lascari, E. Teresi, C. Chiavetta, G. De Luca, A. Irto, C. De Stefano, P. Cardiano, G. Lando, Sustainable recovery of rare earth elements from aqueous media using fruit pomaces: adsorption performance, thermodynamics, and environmental assessment, J. Ind. Eng. Chem. (2025), https://doi.org/10.1016/j.jiec.2025.1009.1008.
[39] L.G. Cançado, K. Takai, T. Enoki, M. Endo, Y.A. Kim, H. Mizusaki, A. Jorio, L. N. Coelho, R. Magalhães-Paniago, M.A. Pimenta, General equation for the determination of the crystallite size La of nanographite by Raman spectroscopy, Appl. Phys. Lett. 88 (2006).
[40] A.C. Ferrari, J. Robertson, Interpretation of Raman spectra of disordered and amorphous carbon, Phys. Rev. B 60 (2000) 14095–14107.
[41] J. Xia, M. Nie, L. Ma, J.R. Dahn, Variation of coulombic efficiency versus upper cutoff potential of Li-ion cells tested with aggressive protocols, J. Power Sources 306 (2016) 233–240.
[42] H. Ohtaki, T. Radnai, Structure and dynamics of hydrated ions, Chem. Rev. 93 (1993) 1157–1204.
[43] L. Castellino, E. Alladio, S. Bertinetti, G. Lando, C. De Stefano, S. Blasco, E. García-España, S. Gama, S. Berto, D. Milea, PyES – an open-source software for the computation of solution and precipitation equilibria, Chem. Int. Lab. Sys. 239 (2023) 104860.
[44] P.M. May, D. Rowland, E. Königsberger, G. Hefter, JESS, a Joint Expert Speciation System - IV: a large database of aqueous solution physicochemical properties with an automatic means of achieving thermodynamic consistency, Talanta 81 (2010) 142–148.
[45] B. Chu, D. Biriukov, M. Bischoff, M. Předota, S. Roke, A. Marchioro, Evolution of the electrical double layer with electrolyte concentration probed by second harmonic scattering, Faraday Discuss. 246 (2023) 407–425.
[46] Y. Zhang, C. Zhu, F. Liu, Y. Yuan, H. Wu, A. Li, Effects of ionic strength on removal of toxic pollutants from aqueous media with multifarious adsorbents: a review, Sci. Total Environ. 646 (2019) 265–279.
[47] P.C. Hiemenz, R. Rajagopalan. Principles of colloid and surface chemistry, revised and expanded, third ed., CRC Press, Boca Raton, 2017.
[48] Y. Bai, R. Essehli, C.J. Jafta, K.M. Livingston, I. Belharouak, Recovery of cathode materials and aluminum foil using a green solvent, ACS Sust. Chem. Eng. 9 (2021) 6048–6055.
[49] J. Pantoja, M. Meléndez-Zaragoza, J. Salinas-Gutiérrez, A. Lopez, Methanol and triethanolamine effect as sacrifice agents in the photocatalytic production of hydrogen over zinc titanates, in: V.R. Pullabhotla (Ed.), Prime Archives in Chemistry, Vide Leaf, Hyderabad, India, 2021.
[50] J.H. Park, Y.S. Ok, S.H. Kim, J.S. Cho, J.S. Heo, R.D. Delaune, D.C. Seo, Competitive adsorption of heavy metals onto sesame straw biochar in aqueous solutions, Chemosphere 142 (2016) 77–83.
[51] J. Shaheen, Y.H. Fseha, B. Sizirici, Performance, life cycle assessment, and economic comparison between date palm waste biochar and activated carbon derived from woody biomass, Heliyon 8 (2022) e12388.
[52] A.S. Mujumdar, Handbook of Industrial Drying, Fourth Edition ed., CRC Press, Boca Raton (USA), 2015.
[53] S. Besseghini, Annual Report on Regulatory Activities and the State of Services, The Italian Regulatory Authority for Energy Networks and Environment, Roma (Italy), 2025.
[54] Y. Shin, S. Kim, S. Park, J. Lee, J. Bae, D. Kim, H. Joo, S. Ban, H. Lee, Y. Kim, K. Kwon, A comprehensive review on the recovery of cathode active materials via direct recycling from spent Li-ion batteries, Renew. Sust. Energy Rev. 187 (2023).
[55] M.A. Abu-Daabes, E. Abu Zeitoun, W. Mazi, Competitive adsorption of quaternary metal ions, Ni2+, Mn2+, Cr6+, and Cd2+, on acid-treated activated carbon, Water (2023) 1070.
[56] A. Ghaemi, M. Torab-Mostaedi, S. Shahhosseini, M. Asadollahzadeh, Characterization of Ag(I), Co(II) and Cu(II) removal process from aqueous solutions using dolomite powder, Kor. J. Chem. Eng. 30 (2013) 172–180.
[57] J.M. Gómez, E. Díez, I. Bernabé, P. Sáez, A. Rodríguez, Effective adsorptive removal of cobalt using mesoporous carbons synthesized by silica Gel Replica Method, Environ. Proc. 5 (2018) 225–242.
[58] H. Hasar, Adsorption of nickel(II) from aqueous solution onto activated carbon prepared from almond husk, J. Haz. Mat. 97 (2003) 49–57.
[59] A.A. Mengistie, T.S. Rao, A.V. Prasada Rao, Adsorption Of Mn(II) ions from wastewater using activated carbon obtained from Birbira (Militia Ferruginea) Leaves, Glob. J. Sci. Front. Res. Chem. 12 (2012) 5–12.
[60] N.Y. Rachel, N.J. Nsami, B.B. Placide, K. Daouda, A.A. Victoire, M.B. Tcheompi, K. J. Mbadcam, Adsorption of Manganese(II) Ions from aqueous solutions onto granular activated carbon (GAC) and modified activated carbon (MAC), Int. J. Innov. Sci. Eng. Technol. 2 (2015) 606–614.
[61] M.N. Siddiqui, B. Chanbasha, A.A. Al-Arfaj, T. Kon'kova, I. Ali, Super-fast removal of cobalt metal ions in water using inexpensive mesoporous carbon obtained from industrial waste material, Environ. Technol. Innov. 21 (2021) 101257.
[62] H. Wang, K. Huang, Y. Zhang, X. Chen, W. Jin, S. Zheng, Y. Zhang, P. Li, Recovery of lithium, nickel, and cobalt from spent lithium-ion battery powders by selective ammonia leaching and an adsorption separation system, ACS Sus. Chem. Eng. 5 (2017) 11489–11495.